Pressure-correction algorithm to solve Poisson system with constant coefficients for fast two-phase simulations

By D. Kim AND P. Moin

1. Motivation and objective

It is a challenging problem to numerically simulate incompressible two-phase flow owing to its complexity and high computational cost. The complexity of two-phase flow are caused by the moving interface between the phases, where density and viscosity abruptly change. Various numerical methods such as the marker method, the volume-of-fluid (VoF) method and the level set method, have been developed to handle arbitrarily shaped interfaces in a fixed grid. Each of these phase tracking methods has its merits and demerits. In the present work, the level set method is used to track the phase interface. The advantages of the level set method is that the topology and movement of the interface are automatically captured. Thus, it is easy to implement numerically. The main drawback of the level set method is that the conservation of liquid volume is not guaranteed. Hybrid methods combining the level set method with VoF Sussman (2000) have been proposed to enhance the mass conservation property. However, the delocalization method has to be used to avoid local curvature error and it makes numerical scheme more complex.

High computational cost is another big issue in turbulent simulations for two-phase flow because it is difficult to apply fast solvers to the Poisson equations. For incompressible two-phase flow, the continuity equation of divergence-free velocity is used to form the Poisson equation for the pressure-correction in the fractional step method. Since the phase interface is moving in time, the coefficients of the Poisson equation is also function of time, while the coefficients is constant in case of single phase flow where density is constant. Because the coefficients of the Poisson equation change in time, the gradient-based method such as the Biconjugate Gradient Stabilized Method is often used instead of the much faster Multigrid method. This results in large extra computational cost since the Poisson solver is the main bottleneck in numerical simulations.

In the present work, a new pressure-correction algorithm is developed to improve the computational speed of the Poisson solver in two-phase flow simulations. In the pressure-correction step, the mass conservation equation or VoF equation is used to obtain the Poisson equation with constant coefficients. Using this method, the mass conservation equation is fulfilled at every time step instead of the divergence-free continuity equation. Since the Poisson equation with constant coefficients is much easier to solve than variable coefficients, the computational speed is much improved. The canonical test problems are solved to demonstrate the accuracy and performance of the method.

2. Governing equations

The governing equations for incompressible, immiscible, two-phase flow are as follows:

$$\frac{\partial \psi}{\partial t} + \nabla \cdot (\psi \mathbf{u}) = 0, \tag{2.1}$$

$$\frac{\partial \mathbf{u}}{\partial t} + \nabla \cdot (\mathbf{u}\mathbf{u}) = -\frac{\nabla \mathbf{p}}{\rho} + \frac{\mathbf{1}}{\rho}\nabla \cdot (\mu(\nabla \mathbf{u} + \nabla^{\mathbf{T}}\mathbf{u})) + \mathbf{g} + \frac{\mathbf{T}}{\rho}, \tag{2.2}$$

where ψ, $\mathbf{u}$, p, μ, and g are the volume of fraction of fluid 1, velocity, density, pressure, viscosity, and gravitational acceleration, respectively. $\mathbf{T}$ is the surface tension force, which acts only on the phase interface ($\mathbf{x_f}$) and vanishes at other locations; it is described as follows:

$$\mathbf{T} = \sigma\kappa\delta(\mathbf{x} - \mathbf{x_f})(\mathbf{n}), \tag{2.3}$$

where σ, κ, δ, and $\mathbf{n}$ are the surface tension coefficient, surface curvature, delta function, and surface normal vector, respectively. The temporal evolution of the phase interface can be predicted by solving the level-set equation:

$$\frac{\partial G}{\partial t} + \mathbf{u} \cdot \nabla \mathbf{G} = \mathbf{0}, \tag{2.4}$$

where the iso-surface of $G = 0$ defines the location of the interface whereas $G > 0$ and $G < 0$ represent two different phase regions, respectively. In the computational domain, G is set to be a signed distance function to the interface such that

$$\mid \nabla G \mid = 1. \tag{2.5}$$

The interface normal vector $\mathbf{n}$ and the interface curvature κ can be calculated from G as

$$\mathbf{n} = -\frac{\nabla \mathbf{G}}{\mid \nabla \mathbf{G} \mid}, \tag{2.6}$$

$$\kappa = \nabla \cdot \mathbf{n}. \tag{2.7}$$

Assuming ρ and μ are constant within each fluid, the density and viscosity are defined as a function of G:

$$\rho = \psi\rho_1 + (1 - \psi)\rho_2, \tag{2.8}$$

$$\mu = \psi\mu_1 + (1 - \psi)\mu_2, \tag{2.9}$$

$$\psi = H(G), \tag{2.10}$$

where the subscripts 1 and 2 denote properties in fluid 1 and 2, respectively, and H is the Heaviside function.

3. Numerical methodology

In the present study, the Refined Level Set Grid (RLSG) method (Herrmann 2008) coupled with a Lagrangian particle-tracking method (Apte *et al.* 2003) is used to capture the phase interface. For the flow solver, an unstructured-grid finite-volume DNS/LES solver named CDP is employed (Ham & Iaccarino 2004; Mahesh *et al.* 2004). The RLSG uses an auxiliary Cartesian grid (G-grid) whereas the CDP uses a base structured or unstructured

grid for fluid flow. Because separate grids are employed in the RLSG and CDP computations, an effective parallel coupling strategy is required for information exchange. The present numerical technique utilizes a coupling infrastructure, called CHIMPS (Alonso *et al.* 2006), to perform the parallel data exchange between CDP and RLSG.

3.1. *Level set transport equation*

In the present study, the velocities u_i^{n+1} is used to advance Eq. 3.1 as

$$\frac{G^{n+3/2} - G^{n+1/2}}{\Delta t} + u_i^{n+1}\frac{\partial G^{n+1/2}}{\partial x_i} = 0. \tag{3.1}$$

The velocities are obtained from CDP and an iterative procedure is needed to solve both $G^{n+3/2}$ and $\mathbf{u}^{n+1}$. This procedure will be explained in section 3.5. The numerical algorithm for the level set transport equation is based on the RLSG method (Herrmann 2008). We use a fifth-order WENO scheme for Hamilton-Jacobi equations (Jiang & Peng 2000) in conjunction with a local Lax-Friedrichs entropy correction (Shu and Osher, 1989). Time integration is performed using a third-order TVD Runge-Kutta method (Shu & Osher 1989).

3.2. *Reinitialization*

Due to numerical errors, the solution of Eq. 3.1 will not preserve G as a signed distance function, i.e., $\mid \nabla G \mid = 1$. Thus, a reinitialization procedure has to be applied to reset G such that $\mid \nabla G \mid = 1$. There are several different methods to reinitialize G. Here, we solve the perturbed Hamilton-Jacobi PDE to a steady state (Chang *et al.* 1995).

$$\frac{\partial G}{\partial \tau} + (V_o - V(\tau))(-P + \kappa)G = 0 \tag{3.2}$$

where V_0 is the total liquid volume at the initial state, and $V(\tau)$ is the liquid mass at pseudo time τ. κ is the local curvature and P is a positive stabilizing constant. Unfortunately, this correction moves the $G = 0$ iso-surface, which is inevitable in a PDE-based reinitialization. However, we can conserve the global mass up to any accuracy depending on the criterion used to achieve the steady state solution. The global mass conservation should be always guaranteed by solving the Poisson equation deduced from the continuity-constraint.

3.3. *RLSG-CDP coupling*

The volume fraction ψ_{cv} of the cell volume V_{cv} is calculated using a step function developed by Van Der Pill *et al.* (2005) as,

$$\psi_{cv} = \frac{1}{V_{cv}} \int_{V_{cv}} H(G) dv. \tag{3.3}$$

The integration is done through CHIMPS. The density and viscosity at the cell center of the cell volume V_{cv} are defined as

$$\rho_{cv} = \psi_{cv}\rho_1 + (1 - \psi_{cv})\rho_2, \tag{3.4}$$

$$\mu_{cv} = \psi_{cv}\mu_1 + (1 - \psi_{cv})\mu_2. \tag{3.5}$$

The properties at the face of the cell volume are computed by averaging two neighboring properties at the cell center. The velocities, u_i, in the level set equation (Eq. 3.1) are interpolated from CDP grid using tri-linear interpolation.

3.4. *Computation of flow fields*

CDP is based on the fractional-step method for collocated variables on unstructured grids, which is especially suitable for large-scale parallel simulations of turbulent flows in complex geometries (Ham & Iaccarino 2004; Mahesh *et al.* 2004). The spatial discretization is performed using a low dissipation second-order central-difference scheme while time integration is performed using a fully implicit Crank-Nicholson method. An upwind-biased scheme is employed to discretize nonlinear terms only at interface cells (Kim *et al.* 2007). The pressure gradient and surface tension forces are predicted by a balanced force algorithm, which guarantees a discrete balance between them (Francois *et al.* 2006; Herrmann 2008). In the following, the new pressure-correction algorithm is presented, which satisfies the mass conservation equation (Eq. 2.1).

The numerical algorithm is

$$\frac{\psi_{cv}^{n+3/2} - \psi_{cv}^{n+1/2}}{\Delta t} + \frac{\partial \psi_{cv}^{n+1/2} u_{i,cv}^{n+1}}{\partial x_i} = 0, \tag{3.6}$$

$$V_{cv} \frac{u_{i,cv}^{*} - u_{i,cv}^{n}}{\Delta t} + \sum_f u_f^{n+1/2} \frac{u_{i,cv}^{n+1/2} + u_{i,nbr}^{n+1/2}}{2} A_f = V_{cv} g + F_{viscous}, \tag{3.7}$$

$$\frac{\rho_{cv}^{n+1/2} u_{i,cv}^{n+1} - \rho_{cv}^{n+1/2} u_{i,cv}^{*}}{\Delta t} = -\frac{\partial p^{n+1/2}}{\partial x_i} + T_{i,cv}^{n+1/2}. \tag{3.8}$$

where A_f is the face area, u_f the face normal velocity, g the gravity, $T_{i,cv}^{n+1/2}$ the surface tension force. The viscous term $F_{viscous}$ is fully implemented and solved in the flux form with the viscosity at the cell face calculated by the harmonic mean of two neighboring viscosities at the cell volumes.

After solving Eq. 3.7 to obtain $u_{i,cv}^{*}$, the cell face normal velocities u_f^{*} are calculated,

$$u_f^{*} = \frac{1}{2}(u_{i,cv}^{*} + u_{i,nbr}^{*}) n_{i,f}. \tag{3.9}$$

Taking the divergence of Eq. 3.8 results in the following Poisson equation,

$$\frac{\partial^2 p^{n+1/2}}{\partial x_i^2} = -\frac{1}{\Delta t}\left(\frac{\partial \rho_{cv}^{n+1/2} u_{i,cv}^{n+1}}{\partial x_i} - \frac{\rho_{cv}^{n+1/2} u_{i,cv}^{*}}{\partial x_i}\right) + \frac{\partial T_{i,cv}^{n+1/2}}{\partial x_i}. \tag{3.10}$$

By using Eq. 3.4 and Eq. 3.6, the mass flux terms in the right hand side become

$$\frac{\partial \rho_{cv}^{n+1/2} u_{i,cv}^{n+1}}{\partial x_i} = (\rho_1 - \rho_2) \frac{\partial \psi_{cv}^{n+1/2} u_{i,cv}^{n+1}}{\partial x_i} = -(\rho_1 - \rho_2) \frac{\psi_{cv}^{n+3/2} - \psi_{cv}^{n+1/2}}{\Delta t}, \tag{3.11}$$

$$\frac{\partial \rho_{cv}^{n+1/2} u_{i,cv}^{*}}{\partial x_i} = (\rho_1 - \rho_2) u_{i,cv}^{*} \frac{\partial \psi_{cv}^{n+1/2}}{\partial x_i} + (\rho_2 + (\rho_1 - \rho_2)\psi_{cv}^{n+1/2}) \frac{\partial u_{i,cv}^{*}}{\partial x_i}$$

$$= -(\rho_1 - \rho_2)\frac{\psi^*_{cv} - \psi^{n+1/2}_{cv}}{\Delta t} + \rho^{n+1/2}_{cv}\frac{\partial u^*_{i,cv}}{\partial x_i}, \tag{3.12}$$

where ψ^*_{cv} is

$$\psi^*_{cv} = \frac{1}{V_{cv}}\int_{V_{cv}} H(G^*)dv. \tag{3.13}$$

G^* is computed from the level set equation as

$$\frac{G^* - G^{n+1/2}}{\Delta t} + u^*_i\frac{\partial G^{n+1/2}}{\partial x_i} = 0, \tag{3.14}$$

Then, Eq. 3.10 is written as

$$\frac{\partial^2 p^{n+1/2}_{cv}}{\partial x_i^2} = \frac{1}{\Delta t}\left\{(\rho_1 - \rho_2)\frac{\psi^{n+3/2}_{cv} - \psi^*_{cv}}{\Delta t} + \rho^{n+1/2}_{cv}\frac{\partial u^*_{i,cv}}{\partial x_i}\right\} + \frac{\partial T^{n+1/2}_{i,cv}}{\partial x_i}, \tag{3.15}$$

and

$$\sum_f \frac{\partial p^{n+1/2}}{\partial n}A_f = \frac{1}{\Delta t}\left\{(\rho_1 - \rho_2)\frac{\psi^{n+3/2}_{cv} - \psi^*_{cv}}{\Delta t}V_{cv} + \rho^{n+1/2}_{cv}\sum_f u^*_f A_f\right\} + \sum_f T^{n+1/2}_f A_f \tag{3.16}$$

in terms of the finite volume formulation, where $T^{n+1/2}_f$ is the face normal surface tension. The surface tension $T^{n+1/2}_f$ at the face is defined,

$$T^{n+1/2}_f = \sigma\kappa^{n+1/2}_f\left(\frac{\partial\psi^{n+1/2}}{\partial x_i}\right)_f. \tag{3.17}$$

Pressure can be solved from Eq. 3.16 by using Multigrid method because it has constant coefficients. Then, the face normal velocity components to satisfy the mass conservation equation (Eq. 3.6) is obtained,

$$u^{n+1}_f = u^*_f - \Delta t P_f, \tag{3.18}$$

where P_f is defined as

$$P_f = \frac{1}{\rho^{n+1/2}_f}(\nabla p^{n+1/2})_f - \frac{1}{\rho^{n+1/2}_f}T^{n+1/2}_f. \tag{3.19}$$

The pressure gradient at the cell center, $P_{i,cv}$ is calculated from the pressure gradient at the cell face, P_f, using the face-area weighted least-squares method (Mahesh et al. 2004) by minimizing

$$\epsilon = \sum_f (P_{i,cv}n_{i,f} - P_f)^2 A_f. \tag{3.20}$$

The velocities at the cell center are finally corrected,

$$u^{n+1}_{i,cv} = u^*_{i,cv} - \Delta t P_{i,cv}. \tag{3.21}$$

In the present method, the velocities at the face do not necessarily satisfy the divergence free equation ($\nabla\cdot\mathbf{u} = \mathbf{0}$). Instead, the mass conservation equation (3.6) is guaranteed by solving Poisson solver.

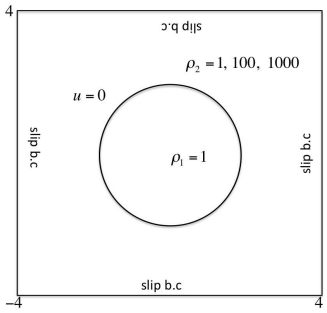

FIGURE 1. Inviscid column at equilibrium.

3.5. *Iteration procedure at each time step*

The iteration process at each time step is followed:

1. Intermediate velocities u_i^* are obtained from the momentum equation.
2. Estimate $G^{n+3/2}$ by solving the level set transport equation using u_i^*.
3. Integrate $\psi_{cv}^{n+3/2}$, $\kappa_{cv}^{n+3/2}$ and transfer to CDP using CHIMPS.
4. Calculate $\rho_{cv}^{n+3/2}$, $\mu_{cv}^{n+3/2}$ from $\psi_{cv}^{n+3/2}$.
5. The corrected velocities u_i^{n+1} and pressure $p^{n+1/2}$ are obtained by solving the Poisson equation.
6. Interpolate u_i^{n+1} on the CDP-grid to G-grid.
7. Repeat the process 2 using updated u_i^{n+1} until convergence.

4. Results

4.1. *Equilibrium inviscid column with exact curvature*

The equilibrium inviscid column is considered in order to demonstrate the balanced force algorithm (Francois *et al.* 2006). As explained in Francois *et al.* (2006), no spurious currents should be produced around a column at equilibrium when the balanced force algorithm is used. Here, we applied the parameters used in Francois *et al.* (2006). A column of radius $R = 2$ is placed at the center of 8×8 domain (figure 1). The surface tension coefficient is $\sigma = 73$ and the theoretical pressure jump across the interface is $\Delta p_{ex} = 36.5$. The densities inside and outside the column are ρ_1 and ρ_2, respectively. The same equidistance Cartesian grid is used for the CDP-grid and G-grid, and the grid size is set to 0.2. Table 1. shows the errors in velocities and pressure after a single time step of $\Delta t = 10^{-6}$ when the exact curvature is used. The errors are machine precision zero even for large density ratios. In the practical simulations, however, the non-zero spurious current is produced because of errors in the curvature calculation.

4.2. *Long-time evolution of the viscous sphere*

In the case of section 4.1, the exact curvature produces machine-zero spurious currents. However, the numerical errors in curvature evaluation result in spurious currents which are small, but non-zero. The long-time behavior of the equilibrium sphere, thus, has been simulated to check errors in velocities after long time steps. A sphere of diameter $D = 0.25$ is placed at the center of a unit sized Cartesian box with Neumann boundary

ρ_1/ρ_2	$L_\infty(u)$	$L_\infty(p_{max} - p_{min} - \Delta p_{ex})$
1	1.06×10^{-17}	4.02×10^{-13}
100	1.87×10^{-17}	5.86×10^{-15}
1000	2.25×10^{-17}	1.93×10^{-15}

TABLE 1. Errors in velocity and pressure after single time step $\Delta t = 10^{-6}$ for different density ratios using the exact curvature.

h, h_G	1/128	1/160	1/192
Ca	5.54×10^{-5}	3.12×10^{-5}	2.21×10^{-5}
Ca (Renardy & Renardy)	3.67×10^{-5}	2.67×10^{-5}	1.59×10^{-5}

TABLE 2. Spurious current capillary numbers of the viscous sphere with those of Renardy & Renardy (2002).

conditions at the sides. The surface tension coefficient is set to $\sigma = 0.357$, density and viscosity in both fluids are $\rho = 4$ and $\mu = 1$. The time step size is $\Delta t = 10^{-5}$. Table 2 shows the maximum spurious current capillary number at $t = 0.002$ compared with Renardy & Renardy (2002). Both methods exhibit good results.

4.3. *Oscillation of column*

The oscillation period for the column without gravity has been performed to verify our method. The theoretical period in the linear regime is given by (Lamb 1945) as

$$w^2 = \frac{n(n^2-1)\sigma}{(\rho_1+\rho_2)R_0^3}. \tag{4.1}$$

A column of radius $R_0 = 2$ is placed at the center of 10×10 domain and the parameters are $\rho_1 = 1$, $\rho_2 = 1000$, $\mu_1 = 0.01$, $\mu_2 = 0.0001$, and $\sigma = 1$. The column is initially perturbed by a mode $n = 2$ perturbation with initial amplitude of $A_0 = 0.01R_0$. The same equidistance Cartesian grid is used for CDP-grid and G-grid. Figure 2 shows the error of the oscillation period with respect to the number of grids. The second order grid convergence is achieved as shown.

4.4. *Broken dam problem*

The well-known broken problem is computed to compare with the experimental result of Martin & Moyce (1952). A water column with $a = 0.06m$ wide and $2a = 0.12m$ high is initially located at rest. The column suddenly breaks down under the gravity $g = 9.81m/s^2$. No slip conditions are applied for all side boundaries. The Cartesian grid of $\Delta = 1 \times 10^{-3}m$ is used here. Figure 3 shows the time history of the phase interface. In

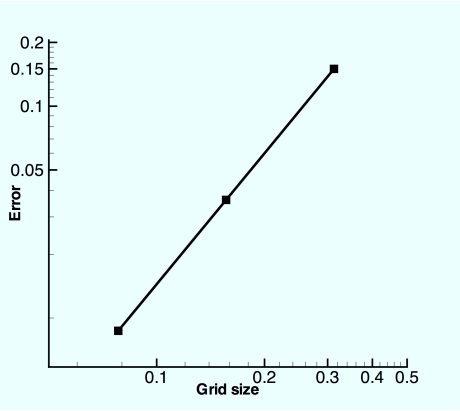

FIGURE 2. Error in oscillation period with respect to the grid size.

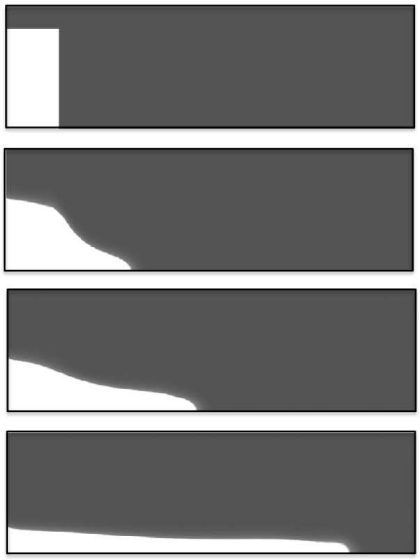

FIGURE 3. Time history of the phase interface in the broken dam problem at the different nondimensional times $t\sqrt{2g/a}$=0, 2.0, 3.0, 5.0.

order to compare with the experimental data (Martin & Moyce 1952), the front position and the height of the column are presented in figure 4. It shows good agreement with the experimental data.

4.5. *Computational performance*

Since the algebraic multigrid method (AMG) can be used for the Poisson solver having constant coefficients, the present method shows much faster performance than the previous method which uses the biconjugate gradient stabilized method (BCGSTAB) for the Poisson solver. Table 3 shows the computational costs measured in CPU seconds per time step on a tetrahedral mesh having 1 million control volumes. In the previous method using BCGSTAB, the level set advection takes only 0.06% of the total time. About 98.8%

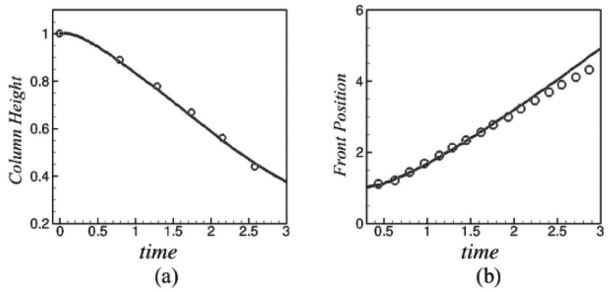

FIGURE 4. (a) time history of the height of the column (b) time history of the front position of the column. —: present result; ○: experimental data (Martin & Moyce 1952)

	Previous method (BCGSTAB)	Present method (AMG)
G advection	0.2	0.8
Reinitialization	1.3	6.3
Momentum solver	2.1	2.5
Poisson solver	310	10.9
Total CPU time	313.6	20.5

TABLE 3. Comparison of computational cost measured in CPU seconds per time step on a tetrahedral mesh of 1 millions.

of the total time step is spent on solving the Poisson equation. However, in case of the present method using AMG, it is more than 10 times faster than the previous method even with several iterations.

5. Conclusions and future work

A new pressure correction algorithm is presented for fast and accurate two-phase simulations. A fractional step method is used to solve the Navier-Stokes equations, and the pressure is used to correct the velocity field to satisfy the mass conservation equation instead of divergence-free velocity. This procedure yields the Poisson system having constant coefficients, which saves computational cost greatly. In the present method, the mass conservation equation is fulfilled at every time step, but the incompressibility is not fully guaranteed due to the numerical errors. These errors can be efficiently reduced by refining the grid. The canonical test problems are solved to demonstrate the accuracy and much improved performance of the method.

The main disadvantage of the present method is that the incompressibility is not fulfilled owing to the numerical errors. In the future, we will focus on reducing or eliminating the errors in incompressibility. Finally, the present method will be used to study air layer drag phenomenon in turbulent flow using more than 500 millions grid points.

Acknowledgments

The work presented in this paper was supported by the Office of Naval Research.

REFERENCES

Alonso, J. J., Hahn, S., Ham, F., Herrmann, M., Iaccarino, G., Kalitzin, G., LeGresley, P., Mattsson, K., Medic, G., Moin, P., Pitsch, H., Schlüter, J., Svärd, M., van der Weide, E., You, D. & Wu, X. 2006 Chimps: A high-performance scalable module for multi-physics simulations. *AIAA Paper* **2006-5274**.

Apte, S. V., Gorokhovski, M. & Moin, P. 2003 Les of atomizing spray with stochastic modeling of secondary breakup. *Int. J. Mult. Flow* **29**, 1503–1522.

Chang, Y. C., Hou, T. Y., Merriman, B. & Osher, S. 1995 A level set formulation of eulerian interface capturing methods for incompressible fluid flows. *Journal of Computational Physics* **124**, 449–464.

Francois, M. M., Cummins, S. J., Dendy, E. D., Kothe, D. B., Sicilian, J. M. & Williams, M. W. 2006 A balanced-force algorithm for continuous and sharp interfacial surface tension models within a volume tracking framework. *Journal of Computational Physics* **213**, 141–173.

Ham, F. & Iaccarino, G. 2004 Energy conservation in collocated discretization schemes on unstructured meshes. *Annual Research Brief* **2004**, 3–14.

Herrmann, M. 2008 A balanced force refined level set grid method for two-phase flows on unstructured flow solver grids. *Journal of Computational Physics* **227**, 2674–2706.

Jiang, G.-S. & Peng, D. 2000 Weighted eno schems for hamilton-jacobi equations. *SIAM J. Sci. Comp.* **21**, 2126–2143.

Kim, D., Herrmann, M. & Moin, P. 2007 Numerical simulation of high shear rate two-phase flow with high density ratio. *Bulletin of the American Physical Society* .

Lamb, H. 1945 *Hydrodynamics*. Dover, New York.

Mahesh, K., Constantinescu, G. & Moin, P. 2004 A numerical method for large eddy simulation in complex geometries. *Journal of Computational Physics* **197**, 215–240.

Martin, J. & Moyce, W. 1952 An experimental study of the collapse of liquid columns on a rigid horizontal plane. *Philos. Trans. R. Soc.* **A224**, 312–324.

Renardy, Y. & Renardy, M. 2002 Prost: a parabolic reconstruction of surface tension for the volume-of-fluid method. *Journal of Computational Physics* **183**, 400–421.

Shu, C.-W. & Osher, S. 1989 Efficient implementation of essentially non-oscillatory shock-capturing schemes. *Journal of Computational Physics* **77**, 439–471.

Sussman, M. & Puckett, E. 2000 A coupled level set and volume-of-fluid method for computing 3d and axisymmetric incompressible two-phase flows. *Journal of Computational Physics* **162**, 301–337.

Van Der Pill, S. P., Segal, A. & Vuik, C. 2005 A mass-conserving level-set method for modelling of multi-phase flows. *Int. J. Numer. Meth. Fluids* **47**, 339–361.